Chaotic Rhythms of a Dripping Faucet

Robert F. Cahalan, Henning Leidecker and Gabriel D. Cahalan

A simple drop detector transforms the computer into a temporal microscope, revealing a variety of rhythms in the common leaky tap

Reprinted from COMPUTERS IN PHYSICS, July/August 1990

Chaotic Rhythms of a Dripping Faucet

Robert F. Cahalan, Henning Leidecker and Gabriel D. Cahalan

A simple drop detector transforms the computer into a temporal microscope, revealing a variety of rhythms in the common leaky tap

The regular beats of a slowly dripping faucet, well-known to the insomniac, give way at higher drip rates to increasingly complex rhythms which aurally express the basic features of chaos. While the interesting rhythms are too rapid to be easily detected by ear, the time intervals can be stored in a personal computer for later playback and analysis. The flow control and drop detector used here were constructed as a school science project. The detector connects to the printer port of an IBM PC, which times the drops to microsecond accuracy with a short program. As the flow rate is increased the time intervals change from periodic to doubly periodic, and finally to various forms of chaos, interrupted by "windows" of periodicity. Several two- and three-dimensional plots of this data are displayed below. One of the simpler plots is approximately parabolic, where each successive time interval is a quadratic function of the preceding interval, with a steepness which depends upon the flow rate. A better approximation adds a small linear dependence on the interval before that, giving a Henon attractor in three dimensions. Such models can be programmed on the computer to simulate dripping faucet rhythms and the sudden rhythm changes which occur as the flow rate increases. At higher rates, the parabola metamorphoses into a zoo of complex and beautiful shapes, still not fully understood, but reproducible by any common tap.

Robert F. Cahalan is a physicist working on the analysis and modeling of the Earth's climate in the Laboratory for Atmospheres at Goddard Space Flight Center in Greenbelt, Maryland. Henning Leidecker is a scientist working in the Materials Branch at Goddard Space Flight Center. Gabriel D. Cahalan is a student at Central High School in Prince Georges County, Maryland, and built the chronoscope and fluid control system described in this article.

Predictability of Fluid Flow

Instability, extreme sensitivity, order in chaos

The complex behavior of the dripping faucet is surprising, in view of the apparent simplicity of the forces involved. The existence of many time scales in a relatively simple fluid system underscores the potential complexity of fluid flow. The ability to predict fluid flow is extremely important in a wide range of problems. The equations of fluid dynamics, which govern fluid flow past sailing vessels, aircraft wings and other solid objects, as well as the motions of the Earth's atmosphere and oceans (which determine the weather and climate), are extensions of Newton's force law to continuous media, and are relatively well-understood. Smooth steady solutions to the equations exist, but in order for a smooth flow to be observed, it must not only obey the equations of fluid dynamics—it must also be stable, so that perturbations in the flow will not grow with time. Our notorious inability to predict flows around aircraft, as well as the evolution of weather and climate, arises because steady flows become unstable as the velocity increases, and these instabilities lead to complex turbulent phenomena.

Complex and unpredictable behavior like that found in fluid turbulence was traditionally thought to involve the interaction of many degrees of freedom, but similar behavior has recently been observed in many relatively simple systems. Poincaré anticipated this a century ago, pointing out that orbits of satellites subject to gravity are, under some conditions, *extremely sensitive to initial conditions*, so that a satellite starting with a position and velocity almost identical to a neighboring satellite would soon find itself far from the other's orbit. Such sensitivity is responsible for the gap structure in Saturn's rings and in the asteroid belt (Wisdom, 1987). In such a situation any small error in the estimated initial position or velocity of a

satellite grows to a large error in the predicted position. Although any single orbit is uniquely determined from the initial position and velocity, such a sensitive orbit is effectively unpredictable, because the initial values cannot be known with infinite precision.

Interest in this kind of behavior has been building over the past quarter century. In 1963 Edward Lorenz found extreme sensitivity to initial conditions in a relatively simple set of three differential equations describing convection in a fluid heated from below. For small heating, the convection occurs in smooth laminar rolls which turn steadily clockwise or counterclockwise. As the heating is increased past a critical value, however, the fluid begins to alternate irregularly between clockwise and counterclockwise, overturning with no predictable pattern. Complex and apparently random behavior has since been found in a variety of simple systems which obey deterministic laws, and so had previously been thought to be quite predictable. At the same time, simple deterministic relationships are being uncovered in systems previously thought to be quite complex because of their apparently random behavior. Simple systems can lead to chaos, and chaos can mask a hidden simplicity.

Logistic equation: period-doubling route to chaos

The dripping faucet experiment, pioneered by Robert Shaw and Peter Scott of the University of California, Santa Cruz, exhibits all the characteristic complexities of chaos in a simple setting. For a certain range of flow rates, the time interval between the nth drop and its successor, T_{n+1}, is found to be determined by the preceding time interval, T_n, through a parabolic relation. The chaotic nature of this so-called "logistic" equation was highlighted in 1976 by R. May in a study of population growth models, where the fraction of the total population capacity obeys a similar rule. The periodic solution, $T_n = T_0$, has a

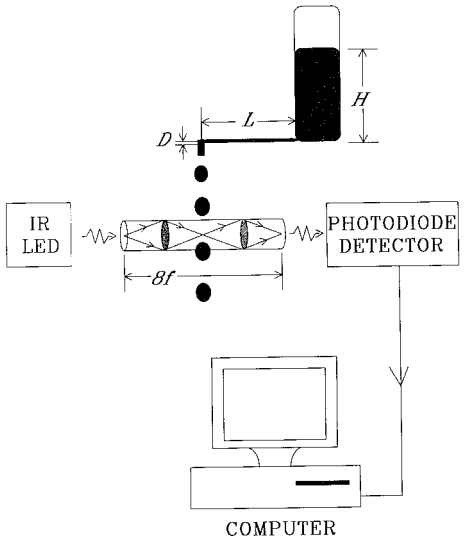

Fig.1: Schematic of dripping faucet experiment. Liquid filling a reservoir to height H passes through a capillary tube of length L and inner diameter D to an eyedropper, from which it drips through a double-lens focusing tube. A beam of light from an infrared LED enters the tube from the left, is focused in the center where it is intersected by the drops, and exits on the right, where it is focused on a photodiode detector. Each drop causes a pulse from the detector to be sent to an IBM PC, which computes and saves the time intervals.

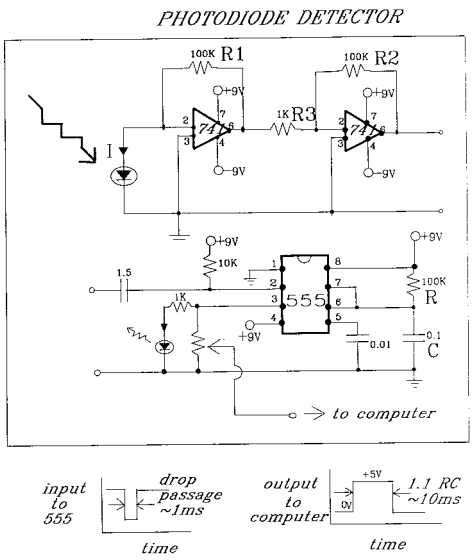

Fig.2: Circuit diagram for the photodiode detector. The beam from the infrared LED creates a current in the photodiode which is amplified by two 741 op amps to a voltage given by IR_1R_2/R_3, which is input to a 555 timer. The timer is configured as a "one-shot", which means that its output, normally OV, suddenly goes "high" when a drop blocks the beam, causing the output LED to flash. The output potentiometer is set so that "high" = 5V, output to pin 11 of the PC parallel port.

stability determined by the slope of the parabola at the periodic point. As the flow rate increases, the parabola steepens, and the magnitude of the slope consequently increases. When it exceeds 1, the periodic solution becomes unstable, and one begins to find an alternating sequence, T_1, T_2, T_1, T_2, and so on, so that drops occur in pairs. This "doubly-periodic" solution becomes unstable at a slightly higher flow rate, and each of the alternating T values becomes an alternating pair, giving a repeating sequence of four different T's. At a still higher flow rate there are eight different T's, and so on. This process of "period-doubling" continues until a critical flow rate, beyond which one finds chaotic behavior (except for "windows" of periodicity at certain flow rates).

Similar chaotic fluctuations occur in a wide variety of systems. Though individual chaotic fluctuations are unpredictable, the period-doubling sequence which leads to chaos has some predictable properties which are largely model-independent, being related to a universal "Feigenbaum constant." In 1980, Mitchell Feigenbaum showed that such transitions occur not only for the parabola, but for a large class of nonlinear functions, and that the parameter values (flow rates) at which the transitions occur have a *universal* relationship independent of the particular model function.

The logistic equation fails to hold at higher flow rates in the dripping faucet, and the droplet time intervals begin to exhibit more complex relationships. In the three-dimensional space with coordinates T_{n+1}, T_n and T_{n-1}, the data lie on various fractal subsets whose complex and beautiful forms were first documented by Shaw and Scott (Shaw, 1984; see also Martien et al., 1985; Yepez et al., 1989; Wu et al., 1989 and Wu and Schelly, 1989). Despite their complexity, these strange fractal forms are reproduced in some detail by the time intervals of drops coming from any common leaky tap. This paper attempts to make this beautiful experiment more widely accessible.

Apparatus and Calibration

A schematic of the experimental apparatus is shown in Fig.1. It consists of five components: (1) a reservoir, in which the liquid is maintained at a constant level, and from which the liquid flows to an eyedropper through a capillary tube of length L and inner diameter D; (2) a cylindrical tube with two identical halves, in which identical lenses are mounted, and which are connected by an adjustable central tube, through which the liquid drips via openings in the side; (3) an infrared LED light source, which supplies light through a small hole in the center of one end of the tube; (4) an infrared photodiode detector, which detects light exiting from a small hole in the center of the opposite end of the tube, and which is connected to pin 11 of the parallel printer port of (5), an IBM-compatible personal computer.

Table 1 gives a list of parts, obtainable at common electronics, plumbing, and office supply stores. Assuming the computer is already available, the system can be built very economically. The simplest working system has been used here, and some enhancements are considered in the concluding discussion.

Table 1. Parts for Time Drop Experiment

½ gallon plastic containers (2)	9V batteries, clamps, clips (3)
car or lab jack	resistors: 1K (2), 10K (1) and 100K (3)
100 cc graduated cylinder	capacitors: 0.01μf, 0.1μf, 1.5μf
capillary tubes: D, L$\approx$1 mm, 10 cm	IR LED source, photodiode detector
eyedropper	741 op amps (2)
rubber tubing, plumber's goop	555 timer
thumbscrew clamp	8-pin IC sockets (3)
dark dye	single-pin sockets
mailing tube	alligator clips (2)
15-watt soldering iron	double-wrapped wire
sponge, glue	heat-shrink tubing
60/40 rosin core solder	25-pin parallel port connector
wire wrap tool, 30 AWG Kynar wire	IBM-compatible personal computer
prepunched perfboard	

Supplying the fluid through a capillary tube, as shown in Fig.1, makes the flow rate vary linearly with the height of the fluid, H. Choosing D$\approx$1 mm ensures laminar flow if H/L is less than about 10, and in that case the volume flow rate, Q, is related to H by Poiseuille's equation,

$$Q = Q_1 H/L, \tag{1}$$

where

$$Q_1 = \pi g D^4/(128\nu) \tag{2}$$

is the rate at H/L = 1. (See for example, Batchelor, pp. 180, 186). When D$\approx$1 mm and $\nu\approx$viscosity of pure water at room temperature (1 cm^2/s), then $Q_1 = 0.24$ cm^3/s. The viscosity of the dyed water used here is a factor of 1.35 larger, giving

$$Q_1 \approx 0.1777 * D^4 \text{cm}^3/\text{s}, \tag{3}$$

where D is expressed in mm. The volume flow rate can be measured at any chosen height by accumulating the volume over, say, one minute. According to (1), a plot of Q versus H/L should produce a linear calibration curve with slope Q_1.

Fig.3a shows two calibration curves for each of two capillary tubes connected to the reservoir and the eyedropper by flexible tubing. Only the fluid height in the reservoir is used, so that the flow rates are shifted up by the pressure drop from the reservoir to the eyedropper. The two on the right are for a capillary tube of length L = 10 cm, and inner diameter D = 0.88 mm. The observed slopes here are 0.1033 and 0.1053, close to the value predicted from (3): $Q_1 = 0.1777*(0.88)^4 = 0.1066$. The intercepts are determined by the vertical height of the capillary tube and eyedropper. In this case they were lowered by 12 cm, shifting the line up by $(12/10)*Q_1$. The two lines on the left are for a capillary tube of length L = 25 cm, and inner diameter D = 1.33 mm. In this case the observed slopes are 0.6209 and 0.5565, compared to the predicted value $Q_1 = 0.1777*(1.33)^4 = 0.5560$, and the tube was lowered 16 cm to shift the line up by $(16/25)*Q_1$.

The program shown in Listing 1 measures the time intervals of 1000 drops, whose sum is the total time, T. The mean drip rate (the number of drops per second) is then

$$r = 1000/T = 1/T_{ave}, \tag{4}$$

where T_{ave} is the average of all the drop intervals. T_{ave} is the average time required for a single drop to fall, so if we knew the average volume per drop, v_{ave}, the volume flow rate would be

$$Q = v_{ave}/T_{ave} = v_{ave} r. \tag{5}$$

In other words, a plot of Q versus r produces a curve whose slope is v_{ave}. When v_{ave} is independent of Q, the resulting plot should be linear.

Fig.3b shows a plot of the volume flow rate versus the mean drip rate for the same runs used in Fig.3a. For flow rates less than about 0.7 cm^3/s, or drip rates in the range 3–7 drops per second, a straight line provides a good fit, and the least-squares slope gives a drop volume of 0.074 cm^3, corresponding to a spherical diameter of 5.2 mm. A second linear fit in the range 7–12 drops per second gives a drop volume of 0.047 cm^3, or a diameter of 4.35 mm. Finally, from 12.5–18 drops per second we obtain 0.015 cm^3, or a diameter of 3 mm, approaching that of the dropper orifice, which is 2.4 mm. Any desired drip rate, or mean time interval, may be obtained by finding the corresponding flow rate from Fig.3b, and then adjusting the fluid level to the required value indicated in Fig.3a.

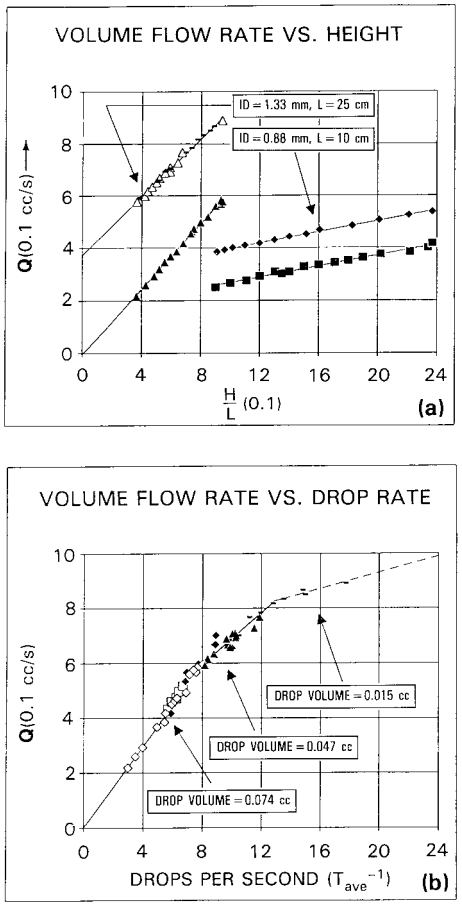

Fig.3: Volume flow rate, Q, in 0.1 cm^3 per second versus (a) fluid height over capillary tube length, H/L, in units of 0.1, and (b) drip rate, which is $r = 1/T_{ave}$, in drops per second. The two callibration curves on the left in (a) are for the capillary tube with length L = 25 cm and with inner diameter D = 1.33 mm, while the two on the right are for the capillary tube with length L = 10 cm and with inner diameter D = 0.88 mm. The slope in (b), determined by least-squares for three ranges of drip rates, gives the average drop volumes: $v_{ave} = 0.074$ cm^3 for r = 3–7 drops/s; $v_{ave} = 0.047$ cm^3 for r = 7–12 drop/s; and $v_{ave} = 0.015$ cm^3 for r = 12–18 drops/s.

Spurious Rhythms

Before discussing true drip rhythms, it is important to recognize the types of errors which can occur in the dripping faucet experiment: (1) systematic error or "drift"; (2) missing or spurious data; (3) random error; and (4) nonstationarity. Examples of each are shown in Figs.4a to 4d, which show "time series" of time interval data versus drop number for four different runs. Excluding 4b and c, in all figures the time interval axis has a range of 50 ms, and the drop number axis has a range of 1000. (Note that unlike conventional time series, these drop measurements do not occur at equally spaced times.) Fig.4a shows a run with systematic drift toward shorter time intervals. Such behavior is associated with changing environmental conditions. For example, the water reservoir's siphon tube drifts to a different position, or a furnace switches on and begins to blow warm air over the experiment, etc. To eliminate drift, the experimental apparatus needs to be stable and isolated from external influences. In the second run (Fig.4b), the detector was not properly aligned with the drop stream, so that a number of drops failed to trigger the detector. When a drop is missed, the measured time interval is the sum of two actual time intervals, or approximately twice the mean time interval. Less frequently, two successive drops may be missed, and the measured time interval is approximately three times the mean. This problem is eliminated by careful beam focusing and alignment. Any spurious time intervals shorter than the mean probably indicate a problem in the detector circuit, or the parallel port.

Fig.4c shows a run with large random variations in the measured time intervals. This could be due to high-frequency environmental vibrations, or to limitations in the experimental apparatus. Random error can be reduced, but only to a lower limit which depends upon the limited accuracy of the measurements, which is related to the size of the drops, the size of the focused beam, the timer resolution, and so on. In practice, if the experimental parameters (flow rate, orifice geometry, etc.) are not too dissimilar to those used here, then it is sufficient to reduce the measurement error to less than ≈ 1 ms in order to observe the fractal patterns of chaos discussed below. The measurement error becomes relatively more important at higher flow rates, and will determine the maximum flow rate at which useful data can be obtained.

Fig.4d shows a run in which the time intervals are nearly constant for more than 300 drops, after which there suddenly appear two different time intervals. This kind of nonstationary time series, in which the statistics suddenly change for no apparent reason, makes both prediction and data analysis very difficult. Such behavior is not due to any experimental error, but is characteristic of chaotic systems. Dynamical models with this kind of behavior are said to be "almost intransitive" (Lorenz, 1975). If the Earth's climate is almost intransitive, then it cannot be uniquely determined by boundary conditions such as the solar constant or atmospheric CO_2 concentration. Such a

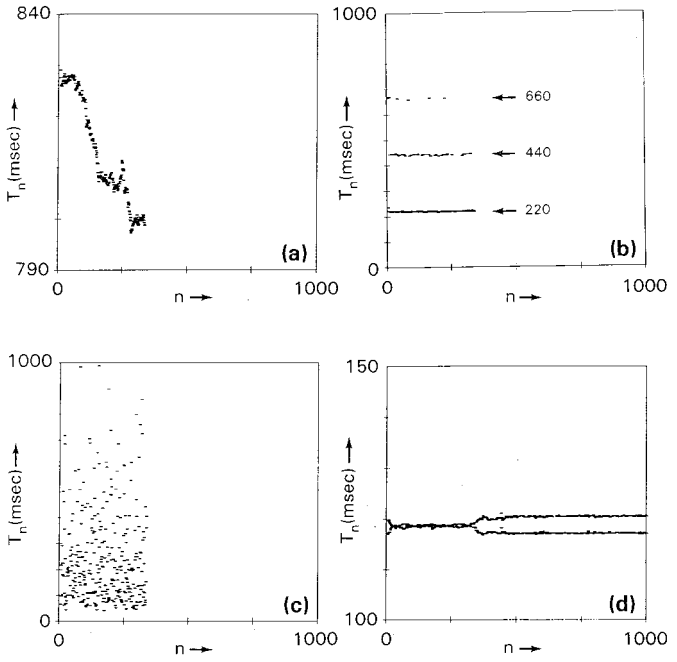

Fig.4: Time interval versus drop number for data containing four types of problems: (a) drift; (b) missing drops; (c) random scatter and (d) nonstationarity.

is always followed by a longer T_{n+1}, and vice versa. Each cloud is elongated and slightly curved due to the transient chaos. Finally, the chaotic drips produce the long curved clouds shown in Figs.6c and 6d, the first appearing smooth and parabolic, while the second, which has been dubbed the "camel," has more structure. The emergence of such orderly curves from the apparently highly random data of Figs. 5c and 5d is quite amazing.

The astonishing implication of these curved clouds is that, to the extent that the small width can be neglected, each time interval is precisely determined by the preceding one, through some function F, such that $T_{n+1} = F(T_n)$. If we had zero measurement error, the timing of every drop could then be predicted from the time interval between just the *first two drops*! Unfortunately, we will

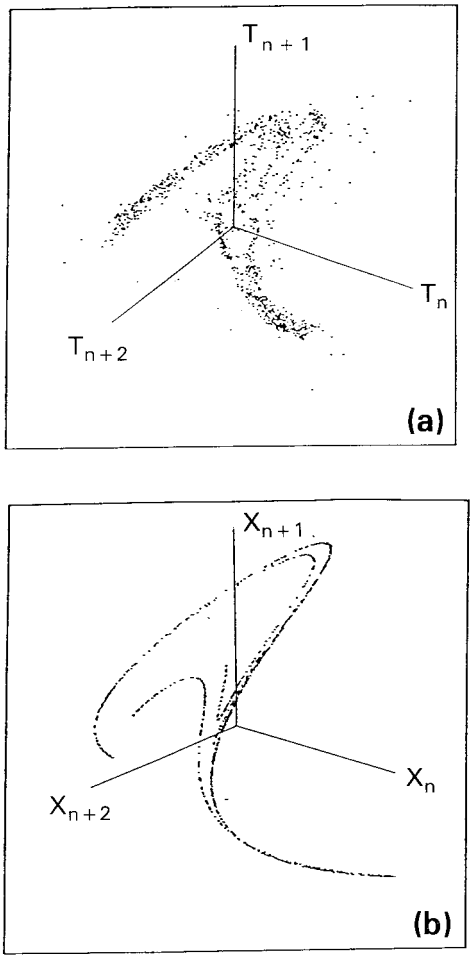

Fig.7: (a) Three-dimensional plot, (T_n, T_{n+1}, T_{n+2}), from data of Fig.5c. Note the 3-stripe ribbon structure. (b) The Henon attractor computed from equation (21), using p=3.45, q=0.345, and displayed in the same three-dimensional coordinates as the water drop data of Fig.7a. Magnification of any of these stripes reveals a 3-stripe substructure, which becomes self-similar at high magnification.

find in the next section that even when F is a simple quadratic function, any initial measurement error, *no matter how small*, rapidly grows larger as more drops fall, until the predicted time interval can appear anywhere in the cloud. So despite the simple relationship described by the function F, the chaotic rhythm can be predicted only for a few drops, while longer-term prediction is no better than a random guess—not unlike our experience with weather prediction. Fortunately, chaos is better than randomness in at least two ways: firstly, some features of the *period-doubling route to chaos* seen in (a) to (c) can be predicted even without detailed knowledge of F, as the next section will discuss; and secondly, chaotic time series can be predicted from initial values for a certain limited *predictability time*, which is estimated for the dripping faucet in the concluding section.

Before moving on to higher flow rates, let's take a closer look at Fig.6c. It would seem to be a parabola, except for the cluster of points which starts just below the peak and extends across the parabola to the right. That would make the function double-valued, so that a drop arriving at an interval of 150 ms could be followed either by one at 146 ms or another one at 150 ms. If the time interval cannot be predicted uniquely from the previous interval, is it enough to give the previous *two* intervals? To find out, we create a three-dimensional scatter plot, using (T_n, T_{n+1}, T_{n+2}) as coordinates, as shown in Fig.7a. (Such plots cannot yet be created with common spreadsheets like Excel. This was done with the Macintosh program "MacSpin.") The extra dimension "uncrosses" the data, so that T_{n+2} is a unique function of T_n and T_{n+1}. Fig.6c is just the projection of Fig.7a onto the plane of (T_n, T_{n+1}) [or equivalently (T_{n+1}, T_{n+2})]. Note that what had looked like a rather complex cloud in two dimensions can now be seen as a double-humped ribbon in three dimensions, with three separate stripes running along its surface. Fig.7b shows a similar three-stripe ribbon generated by adding a linear T_{n-1} term to the parabolic $F(T_n)$, giving the so-called Henon map discussed below. The ribbon in the Henon map may be examined in great detail since one is not limited by measurement error. Each stripe is found to be made of three smaller stripes, and each of these can again be resolved into three smaller ones, and so on. It is a *fractal* ribbon!

Higher Drip Rates

Even as young children, we notice that cloud shapes in the sky often momentarily suggest cars, sheep, camels and a whole zoo of ordinary objects. In the dripping faucet we encounter a zoo of scatter plots as we go to higher flow rates, but unlike real clouds, the animals in this zoo are reproducible in detail, and become quite recognizable once you see them forming in different experiments, although they may appear at different flow rates. Here we look at six examples at increasing flow rates. The time series are shown in Figs.8a to 8f, and the corresponding (T_n, T_{n+1}) plots are shown in Figs.9a to 9f. As in Figs.5 and 6, the axes always cover a time interval range of 50 ms and drop numbers of 1–1000, with precise values given in the figure captions.

We have named the first example, shown in Figs.8a and 9a, the "cobra." Actually, the naming privilege should be reserved for the original discoverers, Shaw and Scott, who found it at a somewhat higher drip rate, as the inset at the upper right in Fig.9a shows. The inset is from Shaw (1984, p. 13) and is centered at 95 ms, with a width of 20 ms. The cobra was observed in the present experiment at $T_{ave} = 123$ ms, or a mean drip rate of 8.1

climate can change without any difference in external conditions, or appear to be steady even when conditions do change. When this occurs in the dripping faucet, it may be necessary to take data for many more than 1000 drops to see clearly what is happening.

Examples of "good" data in each of the three linear regions in Fig.3b will now be described, beginning with the slower drip rates, in the range from 3–7 drops per second. Small changes in the drip rate can produce qualitative changes in the rhythm of the drops, especially for the higher drip rates. These changes may not be evident to the unaided eye or ear, but become quite obvious when plotted as described below. To ensure that all possible types of rhythms are observed, it is important to vary the rate over sufficiently fine intervals, increasing the height by, say, 1 cm in each run. Certain heights may require further investigation after data analysis reveals which rates are of most interest.

Low Drip Rates

Figs.5a to 5d show time series from four runs of gradually increasing flow rate, with mean drip rates of r = 5.70 drops/s, 6.25 drops/s, 6.75 drops/s and 6.80 drops/s. At the slowest rate, case (a), the rhythm of the drop stream is approximately periodic, so that most of the time intervals, with the exception of a few outliers, lie close to the mean interval, with small random deviations. The histogram of the deviations (not shown) approximately follows a normal curve, with large deviations having low probability. The standard deviation depends upon details of the measuring apparatus, and in case (a) it is 0.15 ms, roughly the time needed to read the IBM PC timer.

At slightly higher rates, case (b), the drops begin to arrive in pairs, producing a duple rhythm, so that the time

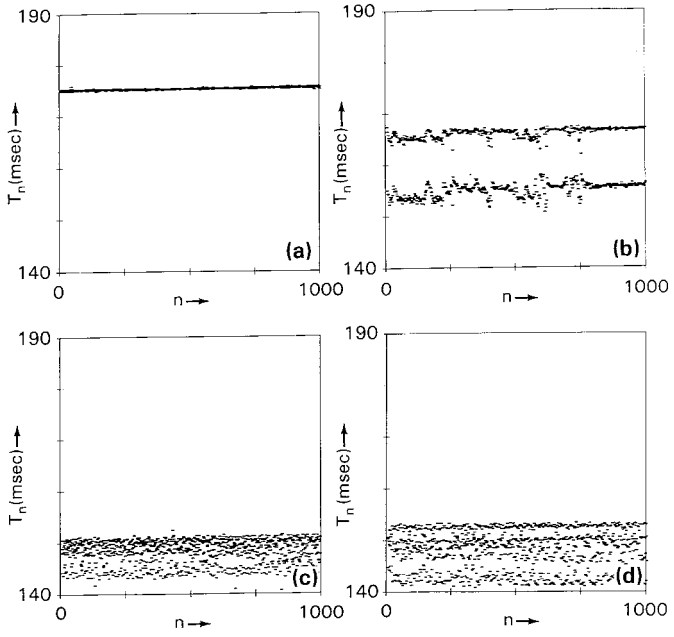

Fig.5: Time interval versus drop number at four low drip rates. The vertical axis covers the range 140–190 ms, and the horizontal 1000 drops. (a) periodic dripping, with a drop every 175 ms, or 5.70 drops/s; (b) biperiodic dripping, with a pair of drops 156 ms apart occurring every 166 ms, or an average interval of 161 ms, or 6.25 drops/s; (c) chaos with an average interval of 148 ms, or 6.75 drops/s; and (d) chaos with an average interval of 147 ms, or 6.80 drops/s.

intervals begin to alternate between a shorter value and a longer value, again with deviations which lie close to each of the two mean values, which are 155.93 ms, with a standard deviation of 0.88, and 166.00 ms, with a standard deviation of 1.25. The larger deviations occur in the first part of the record, and have a more uniform distribution than in case (a). This is due to transient chaos, which dies out by around drop 800, after which the standard deviations reduce to 0.17 and 0.27, respectively.

When the drip rate is again slightly higher, case (c), the drops begin to produce a permanent chaotic rhythm. The mean drip rate here is about 6.75 drops/s, or T_{ave} = 148 ms, but the deviations from the mean, unlike those in (a) and (b), do not tend to lie near the mean, but peak near the maximum positive and negative deviations, with a sharp cutoff outside these values, and a shallow minimum in between. Increasing the drip rate to 6.80 drops/s, or T_{ave} = 147 ms, broadens this bimodal distribution, as seen in case (d).

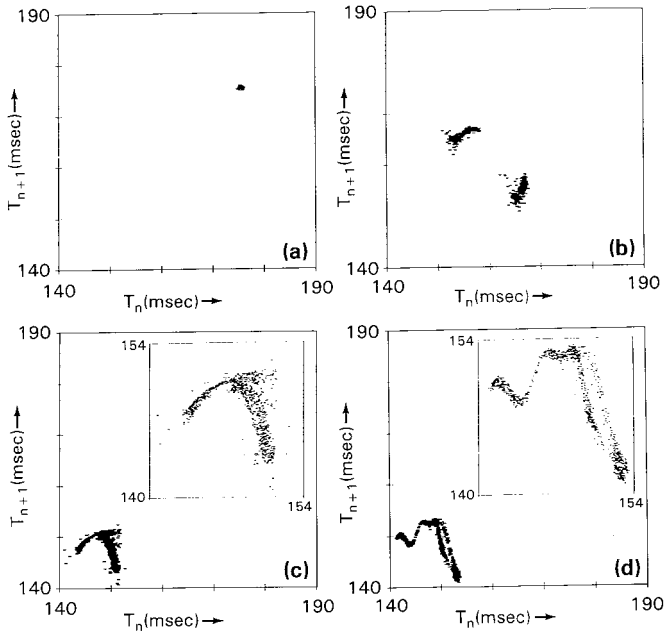

Fig.6: Time interval versus next time interval, (T_n, T_{n+1}), from data of Fig.5. Each axis covers the range 140–190 ms. (a) periodic case from data in Fig.5a; (b) biperiodic case, showing that drop intervals alternate between the two levels in Fig.5b, with variations in each level due to transient chaos; (c) the "parabola" formed by the random-looking data of Fig.5c, with a blowup in the range 140–154 ms; and (d) the "camel" formed by the random-looking data of Fig.5d, also with a blowup in the range 140–154 ms.

Is each time interval in case (c) chosen randomly from the probability distribution, or is it possible to actually predict the successive drop times which produce this chaotic rhythm? To have any hope of predicting, there must be some correlation between one interval and the next. Figs.6a to 6c show scatter plots of (T_n, T_{n+1}) for each of the time series in Figs.5a to 5d. (To reproduce these in Lotus or Excel, copy the data into the second column, but start one row higher. Then make a scatter plot, with column one plotted on the x-axis and column two on the y-axis.) The periodic case, Fig.6a, produces a single cloud of points centered on the mean. The biperiodic case, Fig.6b, produces two separate clouds, so that a shorter T_n

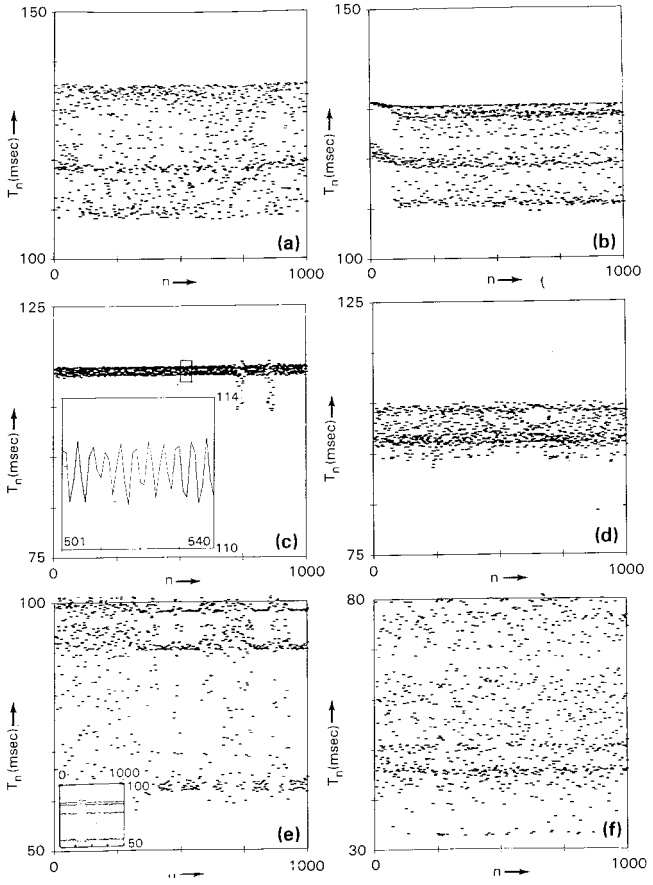

Fig.8: Time interval versus drop number at six higher drip rates. In each case the vertical axis covers a 50 ms range, and the horizontal 1000 drops. (a) chaos at 8.10 drops/s; (b) chaos at 8.17 drops/s; (c) a run in the first periodic window at 8.93 drops/s, with the inset showing time intervals of drops 501–540 with a range 110–114 ms; (d) chaos at 9.82 drops/s; (e) two runs in the second periodic window: triplet rhythm at 11.88 drops/s; with the inset showing a quadruplet rhythm at 13.28 drops/s; and (f) chaos at 17.58 drops/s.

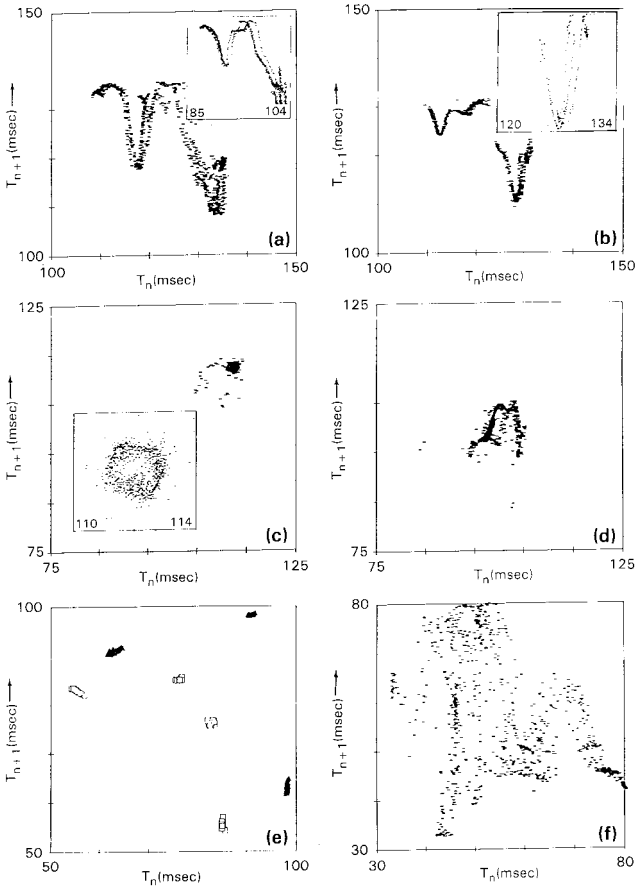

Fig.9: Time interval versus next time interval, (T_n, T_{n+1}), from data of Fig.8. Each axis covers a 50 ms range. (a) the "cobra", with inset reproduced from Shaw (1984); (b) the "adders", with enlarged inset showing the 3-stripe pattern familiar from Fig.7; (c) the periodic modulation seen in the enlarged inset of Fig.8c produces the "ring" seen in this inset; (d) above the first periodic window the chaos is more complex, as in the "ostrich" shown here; (e) in the second periodic window there is intermittent choas, omitted in these composites of the triplet rhythm (solid triangles) and the quadruplet rhythm (open squares); and (f) above the second periodic window, we find the enigmatic "sphinx."

drops/s. Even small-scale details are quite reproducible! Like the parabola, the cobra is double-valued, and appears as a three-stripe ribbon in three dimensions (not shown). The time intervals in Fig.8a are concentrated around three values—110 ms, 117 ms, and 134 ms—so that there is a triple rhythm embedded in the cobra. A clearer period 3 is shown below. In the next section we will see that such triplets are related to a phenomenon called a "tangent bifurcation."

At the slightly higher drip rate of 8.17 drops/s, the cobra is replaced by a brood of smaller snakes, the "adders" of Figs.8b and 9b. The usual three-stripe pattern appears again, as shown in the inset in 9b, which is a blowup of the right side. The breakup of the cobra into these smaller structures as the rate increases is a kind of "reverse" bifurcation—the opposite of the sequence seen at lower rates (Figs.6a–6d). As the rate continues to increase to 9–10 drops/s, a periodic "window" occurs. An interesting example is the "ring" shown in Figs.8c and 9c, at a rate of 8.93 drops/s, or $T_{ave} = 112$ ms. The inset in 8c, which shows a blowup of 40 drop intervals from the middle of the ring's time series, reveals a rapid oscillation over a range of about 2 ms. The power spectrum of this oscillation (not shown) has a sharp spike at a period of 3.55 drops, or about 398 ms. This slow 398 ms modulation of the 112 ms period leads to the circle shown in the inset in 9c, which is a kind of Lissajous figure for the drop stream. This kind of behavior was also observed by Wu et al., (1989).

The periodic window ends at about 100 ms, below which more complex chaos appears, some with loops such as the "ostrich" of Figs.8d and 9d, or the "eagle" observed by Shaw et al., or with multiple hills and valleys. There follows another periodic window with a triplet rhythm, as shown in Figs.8e and the solid triangles in 9e. This is a prime example of the phenomenon of "intermittency," observed in all kinds of fluid turbulence, in which periods of smooth periodic behavior are interrupted by irregular bursts of chaos. This example shows 5 time periods with the triplet periodic rhythm, separated by 6 time periods during which the rhythm is chaotic. The triplet periodic points are plotted as solid triangles in Fig.9e. More chaos occurs at flow rates above the triplet window, followed by a third periodic window. An example here is the quadruplet rhythm shown in the inset in Fig.8e. This example also exhibits intermittency, as in the triplet case.

x = half the vertical height of the clock hand below 12 o'clock, then

$$x_n = [1 - \cos(2\pi A_n)]/2. \quad (9)$$

Substituting (9) and p = 4 into the logistic equation gives

$$[1 - \cos(2\pi A_{n+1})]/2 = [1 - \cos(2\pi A_n)] \times [1 + \cos(2\pi A_n)] = [1 - \cos(4\pi A_n)]/2$$

where on the right side we used the trigonometric identity $(\cos(2\pi A))^2 = [1 + \cos(4\pi A)]/2$. Comparing the left and right sides, we see that

$$A_{n+1} = 2A_n \mod 1. \quad (10)$$

Here mod 1 means to drop the integer part of A, and keep just the fractional part. Since each iteration doubles A, the initial angle A_0 gets doubled *n times* to get A_n. This completely solves the logistic equation. For any x_0, we can compute the initial angle by solving (9) for A_n, and setting n = 0 to get

$$A_0 = [\cos^{-1}(1 - 2x_0)]/(2\pi). \quad (11)$$

We then find the complete sequence of angles from A_0 using the following:

$$A_n = 2^n A_0 \mod 1. \quad (12)$$

Finally, we substitute these into (9) to get the sequence of x_n. So all the x_n are precisely determined from x_0.

As a simple example, start with $x_0 = \frac{3}{4}$ in (11). Then $1 - 2x_0 = -\frac{1}{2}$, and since $\cos^{-1}(-\frac{1}{2}) = 120° = 2\pi/3$ radians, we get $A_0 = 1/3$, so the clock hand is at 4 o'clock. Doubling A_0 gives $A_1 = 2/3$, moving the hand to 8 o'clock. Then from (9) we get $x_1 = [1 - \cos(4p/3)]/2 = \frac{3}{4}$. Although A has doubled, x is unchanged, since 4 o'clock and 8 o'clock have the same vertical height. Doubling A again gives 4/3, but only the fractional part matters, so $A_2 = 1/3$, which puts us back at 4 o'clock, and again $x_2 = \frac{3}{4}$. So the angles alternate: A = 1/3, 2/3, 1/3, 2/3, or 4 o'clock, 8 o'clock, 4 o'clock, 8 o'clock, and so on. Apparently it's either teatime or bedtime! The height of the hand (representing the drop time intervals) is apparently stuck at a fixed point: $x = \frac{3}{4}$, $\frac{3}{4}$, $\frac{3}{4}$, $\frac{3}{4}$, and so on. This fixed point agrees with x_0* found by substituting p = 4 in (8). However, in order for this solution to actually be observed, it must also be stable, so that perturbations will not grow with time.

To investigate stability, we shall use a calculator as a digital clock. Calculating the sequence of angles from equation (10) is simple arithmetic, and can be done by hand. But let's suppose for a minute that equation (10) is as complicated as weather prediction equations, and we have to compute it with a calculator, again starting at $A_0 = \frac{1}{3}$. Calculators, even big computers, do not know fractions. So the computer will have some approximation to 4 o'clock, say $A_0 = 0.333$. Let's follow it for the first 12 computations of equation (10): $A_1 = 0.666$, $A_2 = 0.332$ (dropping the 1), $A_3 = 0.664$, $A_4 = 0.328$, $A_5 = 0.656$, $A_6 = 0.312$, $A_7 = 0.624$, $A_8 = 0.248$, $A_9 = 0.496$, $A_{10} = 0.992$, $A_{11} = 0.984$, $A_{12} = 0.968$. Even though the initial error was only about 0.1%, after 10 steps the

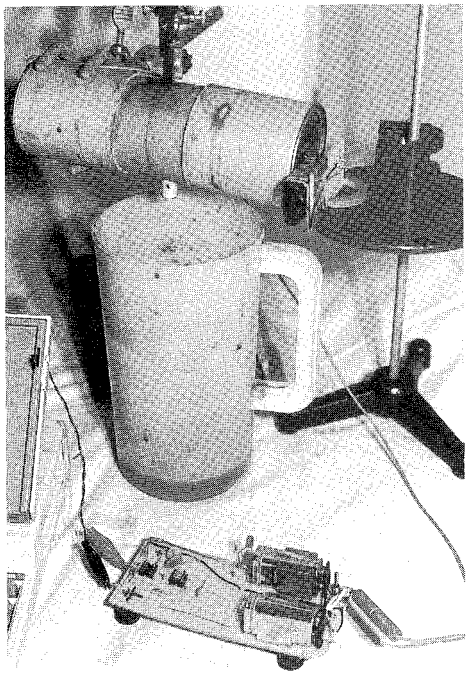

Drops from the eyedropper drip through the 2-lens focusing tube shown here, where they block an infrared beam from the source circuit at right. The drop in intensity detected at the photodiode on the left of the tube is amplified and converted to a digital pulse by the circuit at bottom (Fig.2), which is then sent to the parallel port of an IBM-compatible computer (here a T1000 laptop), where data are accumulated by the C program in Listing 1.

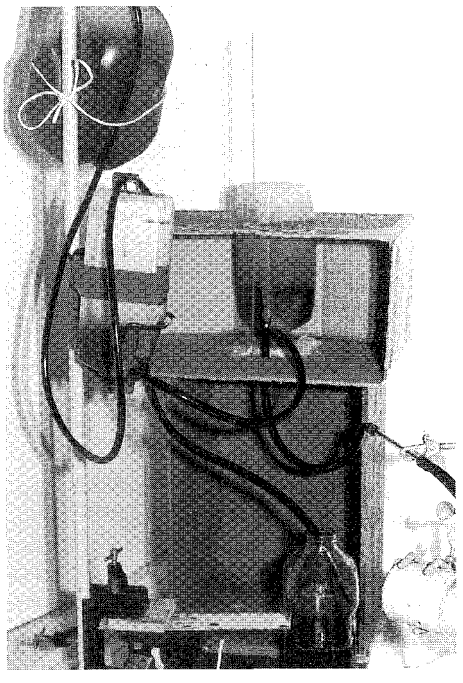

The fluid flow is controlled by siphoning it from a tank (here a gallon container at upper left) to an overflow reservoir mounted on a jack, and then to a fixed reservoir, where the fluid height is varied by adjusting the jack, and finally through a horizontal capillary tube (at right center) to the eyedropper.

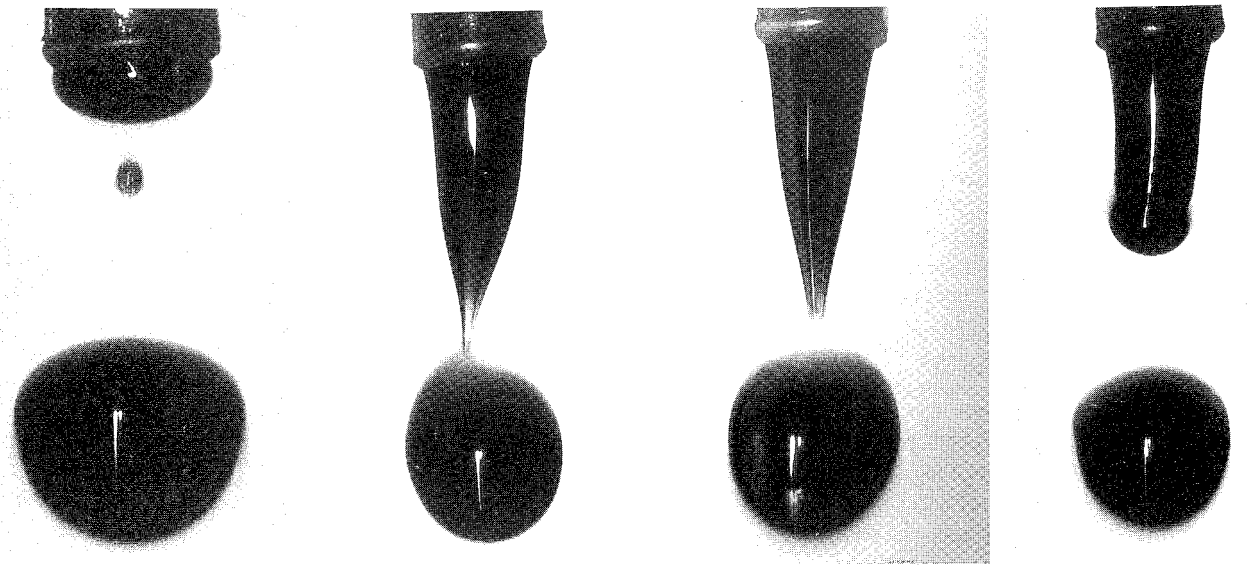

Drops emerge from the eyedropper at a few per second. The larger one, about 3.34 mm in diameter, has an oscillation period of about 18 ms. The small satellite drop left by the recoiling fluid column, about 0.5 mm in diameter, may be missed by the detector. Its oscillation period is about 1 ms, so that it completes roughly one cycle during the exposure time of the picture. The remaining three photos show stages in the recoil of the water column. Note the capillary waves on the column's surface in the photograph at far right.

predictions are 100% wrong, and the clock has started to tick erratically! The error has grown by a factor of 1000 in 10 ticks!

The calculated values initially move away from the fixed point at $x_0^* = \frac{3}{4}$ because it is unstable, but why does the chaos continue when the clock is not near that point? Let us investigate the behavior at some other point, not a fixed point. Let's just start the clock at some random instant, and since irrational numbers are more common than fractions, let's choose $A_0 = 2^{-\frac{1}{2}} = 0.707$. It is easiest to see what happens if instead of using decimals (tenths, hundredths, thousandths, and smaller powers of ten) we expand A_0 in binary (halves, fourths, eighths, and smaller powers of two). If our calculator has 8-bit accuracy (although most have 80 bits), then we have $A_0 = 0.1011\ 0100$. Multiplying by two just changes halves to ones, fourths to halves, and so on, which has the effect of shifting each bit one place to the left, like multiplying by 10 in decimal. The bit that crosses the decimal point gets dropped, since we keep only the fractional part. This action of equation (10) on the bits of A is a *Bernoulli shift*. Applying this shift to A_0 gives $A_1 = 0.0110\ 100b_1$, where a new bit, b_1, has appeared. Its value is related to the roundoff error of the calculator. As we continue to apply the Bernoulli shift, the bits present in A_0 are shifted past the decimal point and stripped off one by one, and more error bits get shifted toward the decimal point, until no memory of the initial angle remains, and further predictions are based only on roundoff error. This will occur for any choice of A_0, so we can conclude that every point is unstable when $p = 4$. As a result, the logistic equation becomes a random number generator!

What is the probability distribution of these random numbers? Imagine setting each of 100 clocks to a random time by spinning the hand like a fortune wheel. Assume any initial time is equally probable, so approximately half the clocks are between 12 and 6, with $0 < A_0 < \frac{1}{2}$, and half are between 6 and 12, with $1/2 < A_0 < 1$. This is a *uniform* distribution. At the first tick the times are doubled, and so the angles of the first group stretch over the range $0 < A_1 < 1$, uniformly throughout the circle. Doubling the angles of the second group moves them into the range $1 < A_1 < 2$, but only the fraction matters, so that group of clock angles is also spread uniformly over $0 < A_1 < 1$. In other words, a uniform distribution of angles is unchanged by a Bernoulli shift, and it is therefore called the *invariant distribution* of the Bernoulli shift. Any other initial distribution of angles eventually evolves toward the uniform invariant distribution. What distribution of x is implied by the uniform distribution of angles? Probability

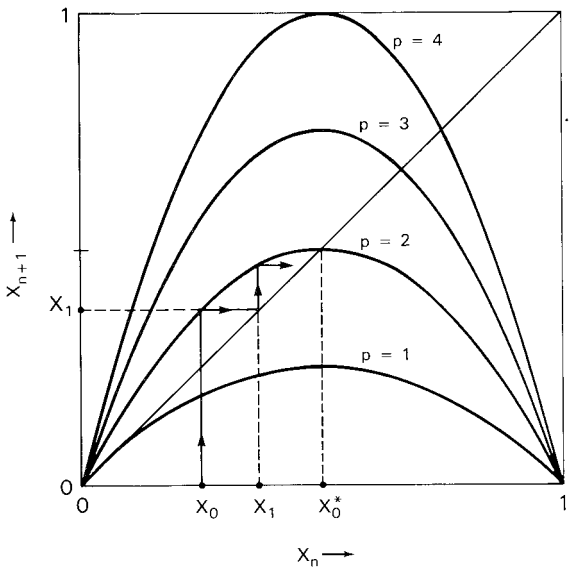

Fig.10: Plots of parabola $f(x) = px(1-x)$ for $p = 1, 2, 3$ and 4. Note that the maximum occurs at $x = \frac{1}{2}$, and has the value $p/4$. The graphical method of iterating the logistic equation is shown for $p = 2$: starting at the initial point $x = x_0$, we go vertically to the curve, then horizontally to the line, which gives $x = x_1$, then iterate by repeatedly going vertically to the curve and horizontally to the line. When $p = 2$, this eventually leads to the "fixed point" $x = x_0^*$, where $f(x) = x$.

theory tells us that the answer is inversely proportional to the derivative of (9),

$$\text{probability}(x) = [dx/dA]^{-1}. \tag{13}$$

Some calculus shows that the derivative, dx/dA, is small near $x = 0$ and $x = 1$, so the probability becomes large near these two points, and has a minimum in between, which agrees with the observations in Figs.6c and 6d.

Now let us return to the cases for which p is between 2 and 4. Recall from Fig.10 that at $p = 2$ the solution approaches the stable fixed point at $x_0^* = \frac{1}{2}$, where the slope of f is zero. As p increases to 3, the peak of the parabola moves up, x_0^* moves to the right to $\frac{2}{3}$, and the tangent to the curve at x_0^* approaches 45° from the horizontal, where the slope equals -1. Fig.12 graphically demonstrates the *slope-stability theorem*: fixed points at which the curve is

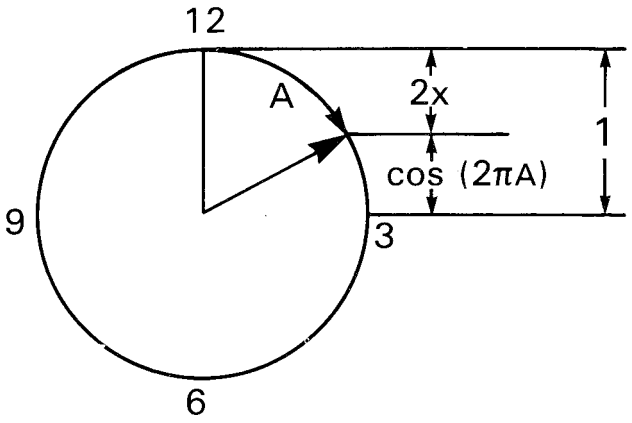

Fig.11: Interpretation of the change of variables given in equation (9). The clock radius is 1, and the angle A measures the fraction of circumference between the clock hand and 12 o'clock.

45° or steeper (i.e. the magnitude of the slope exceeds 1) are unstable, but those with lower slopes are stable. The slope at x_0^* can be computed by taking the derivative of (6) and substituting (8). That gives

$$\text{slope} = 2 - p. \tag{14}$$

This slope becomes equal to -1 when p becomes equal to $p_1 = 3$, where $x_0^* = \frac{2}{3}$. Fig.13a shows what happens slightly above p_1. No matter where we start, eventually an alternating sequence, or two-cycle is produced: the sequence $x_0, x_1, x_2, \ldots$ eventually becomes $x_1^*, x_2^*, x_1^*, x_2^*, \ldots$. That means that *two* applications of the logistic equation bring us back to the same point, so instead of the fixed point condition of (7), we now have

$$x^* = f(f(x^*)) = f_2(x^*). \tag{15}$$

where the function f_2, shown in Fig.13b, is the *second iterate* of f, defined as $f_2(x) = f(f(x)) = p[f(x)]\,(1 - [f(x)]) = px(1 - x)\,(1 - px(1 - x))$. If $x^* \neq 0$, then x^* can be divided out of (15), leaving a cubic equation with three solutions which determine the three nonzero locations where f_2 intersects the line in Fig.13b. The central fixed point of f_2 is identical to x_0^*, the fixed point of f, since one solution of (15) is obtained by setting $f(x^*) = x^*$. The other two fixed points of f_2 form the two-cycle of f.

The stability at each fixed point of f_2 is determined by the slope at each point. The slope of f_2 is related to the slope of f by a simple product rule:

$$\text{slope of } f_2 \text{ at } x_n = (\text{slope of f at } x_n) \times (\text{slope of f at } x_{n+1}), \tag{16}$$

which comes from the chain rule for derivatives. If we apply the rule at the central fixed point of f_2 (which is also the fixed point of f), we can use $x_{n+1} = x_n = x_0^*$, so the rule tells us that

$$\text{slope of } f_2 \text{ at } x_0^* = (\text{slope of f at } x_0^*)^2. \tag{17}$$

This implies that when the slope of f at x_0^* becomes steeper than -1 (i.e. as p increases past p_1) then the slope of f_2 at x_0^* simultaneously becomes steeper than $+1$. So below p_1, f_2 has only one stable fixed point (at x_0^*), but it becomes unstable as p passes p_1, when x_1^* and x_2^* appear. This splitting of one stable fixed point into one unstable and two stable fixed points is called a *pitchfork bifurcation*. If we apply rule (16) at $x_n = x_1^*$, we can use $x_{n+1} = x_2^*$, and if we apply it at $x_n = x_2^*$, we can use $x_{n+1} = x_1^*$, so in either case we get the same product (slope of f at x_1^*) times (slope of f at x_2^*), so that

$$\text{slope of } f_2 \text{ at } x_1^* = \text{slope of } f_2 \text{ at } x_2^*. \tag{18}$$

In other words, both points of the two-cycle have the same stability. As p continues to increase in Fig.13b, the slopes at x_1^* and x_2^* will reach zero when $x_1^* = \frac{1}{2}$, and as the curve steepens, x_1^* will move below $\frac{1}{2}$ while x_2^* will move toward 1, and both slopes will approach -1, where the two-cycle will become unstable. We label that value $p = p_2$, and just as the fixed point of f becomes a two-cycle

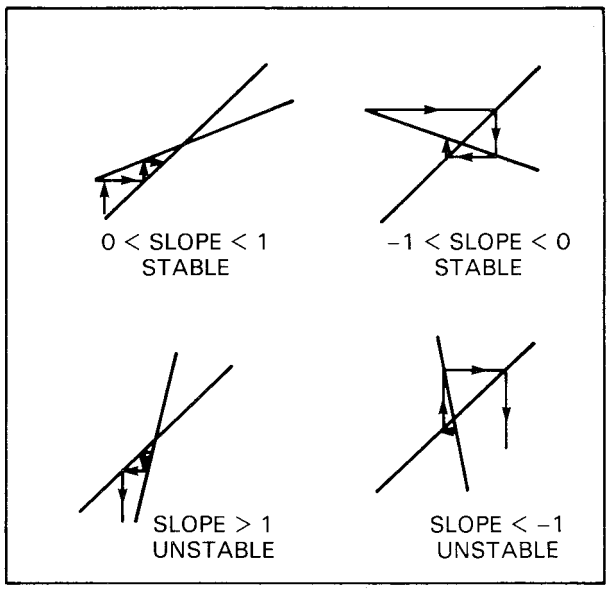

Fig.12: Illustration of the "slope-stability" theorem at a fixed point: (a) steady approach to the fixed point for slopes positive and less than 1; (b) spiral approach for slopes negative and greater than −1; (c) steady retreat from the fixed point for slopes greater than 1; and (d) spiral retreat for slopes less than −1.

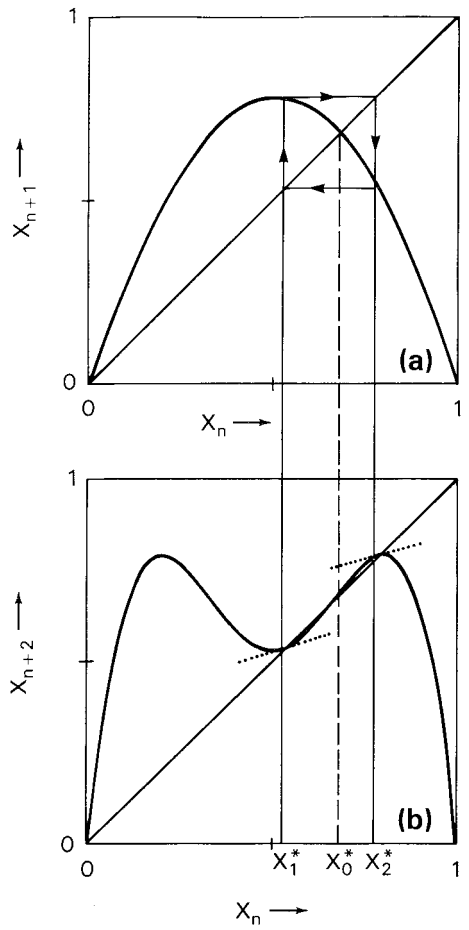

Fig.13: Relationship of f(x) (upper curve) and $f_2(x)=f(f(x))$ (lower curve). The unstable fixed point of f is also an unstable fixed point of f_2, while the 2-cycle of f corresponds to 2 stable fixed points of f_2, both having the same slope.

at $p_1 = 3$, each fixed point of f_2 becomes a two-cycle at the higher value of $p_2 = 3.448$. The pair of two-cycles of f_2 correspond to four fixed points of f_4 (the fourth iterate of f) and the chain rule again implies that all four have the same stability. The logistic equation has a stable four-cycle just above this second period doubling at p_2, and as p continues to increase, the four-cycle becomes unstable and is replaced by a stable eight-cycle at $p_3 = 3.544$, and so on.

Feigenbaum (1983 and references therein) has studied the limiting behavior of the period-doubling sequence. Each period-doubling occurs after a shorter interval of p. If p_n is the value at which the period doubles for the nth time, the ratio of each interval $p_{n+1} - p_n$ over the next one approaches a number called the Feigenbaum constant:

$$(p_{n+1} - p_n)/(p_{n+2} - p_{n+1}) = 4.66920166..., \qquad (19)$$

Amazingly, this constant is *universal*, so that *any* function with a single smooth maximum undergoes period-doubling at this same rate. As $n \to \infty$, p_n approaches the value

$$p_\infty = 3.56994567.... \qquad (20)$$

At p_∞ *every* cycle of period 2^n becomes unstable, and x begins to hop around on a fractal set of points—the onset of chaos. This fractal set is called a *strange attractor*, and like the Feigenbaum constant, it is universal—as long as f(x) has a single smooth maximum, x follows the same orbit at p_∞ no matter what f(x) is!

The complete behavior of the logistic equation can be summarized by its *bifurcation plot*. Fig.14a shows a portion of it computed from numerical solutions of the logistic equation in the range $3 \leqslant p \leqslant 4$. For each p along the horizontal axis, (6) was iterated starting at $x_0 = 2/3$, the first 5000 values were discarded, and the rest were plotted on the vertical axis. The first 4 period-doublings are visible at $p < p_\infty$, followed by bands of chaos at $p > p_\infty$, which gradually widen and merge until the full range of x is covered at $p = 4$. Windows of periodicity are visible in the chaotic region, the widest having 3 values of x—a triplet of period 3. If we expand the region around the largest triplet value, we obtain Fig.14d, where the scale has been expanded by a factor of 0.016. This tiny part is similar to the full set, and has its own triplet window. Clearly this expansion process could continue indefinitely. Such a set which has complex structure at any magnification is called a *fractal* (Mandelbrot, 1983).

Sarkowskii's theorem, often stated as "period 3 implies chaos," tells us that there are windows of every other integer period to the left of the triplet window in Fig.14, and the theorem gives the order of the periods. (For a simple proof, see Kaplan, 1987). The period 3 window begins at $p = p_c = 2\sqrt{2} + 1 = 3.828427...$, where $f_3(x)$ is tangent to the $x_{n+1} = x_n$ line at three locations, as shown in Fig.15a. When p exceeds p_c, the curve crosses the line, producing a stable and an unstable fixed point at each location. This is called a *tangent bifurcation*. When p is slightly less than p_c, then the curve will be slightly above the line, similar to what was observed with the cobra in Fig.8a. In this pre-bifurcation situation the neighborhood of the near-tangency behaves like a pinched hose, as shown in Fig.15b. Many iterations are required in order to pass through the pinched region. This leads to the often-observed phenomenon of "intermittency," in which periods of chaos alternate with apparently periodic behavior. This is responsible for the denser regions in the chaos just to the left of the period 3 window in Fig.14a, and also accounts for the three peaks in the histogram of the cobra.

Finally, consider what happens when (6) begins to break down, so that x_{n+1} depends not only on x_n, but on earlier intervals as well. Such dependence was observed not only for the cobra and dragon, but even for the parabola, where the three-dimensional view seen in Fig.7 reveals a three-striped ribbon. Perhaps the simplest generalization of the logistic equation is the Henon map, one form of which is

$$x_{n+1} = f(x_n, x_{n-1}) = px_n(1 - x_n) + q(x_{n-1} - \tfrac{1}{2}). \qquad (21)$$

As q approaches zero, the dependence on x_{n-1} goes away and we get the logistic equation again. Fig.7b shows an orbit of this equation computed with $p = 3.45$ and $q = 0.345$, and plotted with the same axes as in Fig.7a. The details are different from Fig.7a, but the general shape is similar, and three stripes are visible. On closer inspection the rightmost stripe resolves into three closely

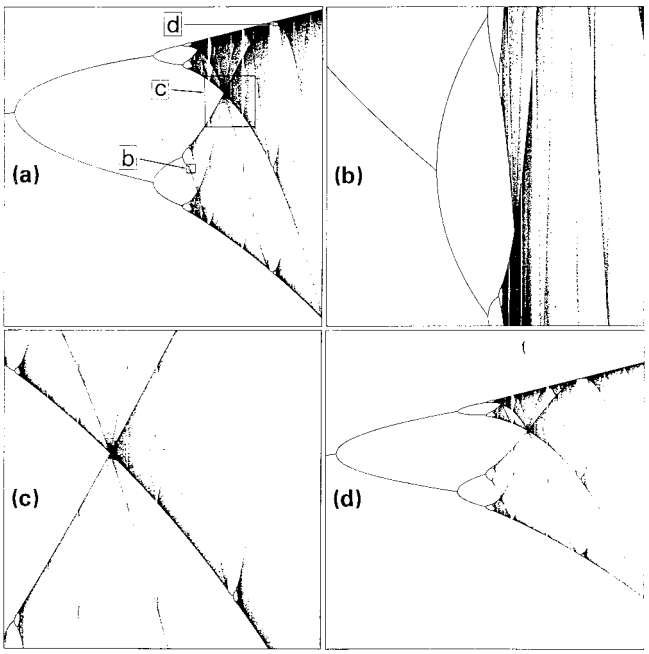

Fig.14: Stable attractor values of x on the vertical axis as a function of the control parameter p on the horizontal (a so-called bifurcation plot). The upper left region (a) shows the complete plot beginning at the first bifurcation, (2.97,0) to (4.0,1), and the other three regions show the following subwindows: (b) the onset of chaos: (3.555, 0.4775) to (3.582, 0.5045); (c) the central intersection of chaotic bands: (3.625, 0.630) to (3.785, 0.790); and (d) the top branch of the triplet window: (3.841, 0.950) to (3.857, 0.966).

spaced stripes, and if we continue to zoom in, more and more stripes are resolved. Again we have a fractal set. Zooming in on the turning point at the top of the figure produces an image that looks similar to the rings of Saturn (see p. 53 of Crutchfield et al., 1986).

Faucet Physics

Imagine a pendant drop, hanging at rest on the tip of the faucet or eyedropper. The force of gravity gives the drop weight, and pulls it down, but this is balanced by cohesive forces which create surface tension, holding the drop together and pulling it back toward the column of fluid in the eyedropper. If the flow rate is small, but nonzero, the mass of the drop slowly increases, stretching the drop downward. When the drop is small, surface tension tends to make it round, but as it grows, gravity increasingly elongates it. Gravity becomes important as the drop's length exceeds the meniscus constant $(\sigma/\rho g)^{\frac{1}{2}} \approx 2.5$ mm, after which the drop forms a neck, which gradually closes off its connection with the fluid above, until it breaks off and begins to fall. As the drop falls, it oscillates about a shape approximately spherical, and the water column rebounds and oscillates about an equilibrium position, until friction with the walls slows it to rest, after which the small flow rate begins to form a new drop. When the flow rate is small enough, the motion of the fluid is unimportant, and the mass of the drop at the breaking point is purely an equilibrium problem, which may have a complicated dependence on properties of both the water and the eyedropper, but will be the same for every drop. In that case, each drop will have the same mass, and therefore take the same amount of time to form, resulting in the slow periodic rhythm so torturous to those striving toward sleep.

The situation is much different at higher flow rates. Then the breaking point occurs when the fluid is still oscillating from the previous drop. There is a resonance between the forcing frequency, which is the drop formation time, and the natural oscillation frequency of the water column. The natural oscillation frequency of a single drop can be computed from Rayleigh's formula, which for the lowest mode in pure water has the form $f = 11d^{-1.5}$ (Nelson and Gokhale, 1972), where d is the drop diameter in cm. For the 5.2 mm drops observed here, that gives about 30 cycles/s—too high to explain the observation of chaos at less than 10 drops/s. The natural frequency is inversely proportional to the square root of the mass, so the oscillating mass of fluid in the eyedropper is evidently about 10 drop masses.

At higher flow rates, then, the drop's mass depends upon the column's motion, which depends upon the previous drop's mass, which depends upon the previous motion, and so on. While this sounds very difficult to model, the fact that many different faucets produce the same set of rhythms (period doubling, the parabola, cobra, dragon, etc.) gives us hope that a highly simplified model might capture the essential physics of the dripping

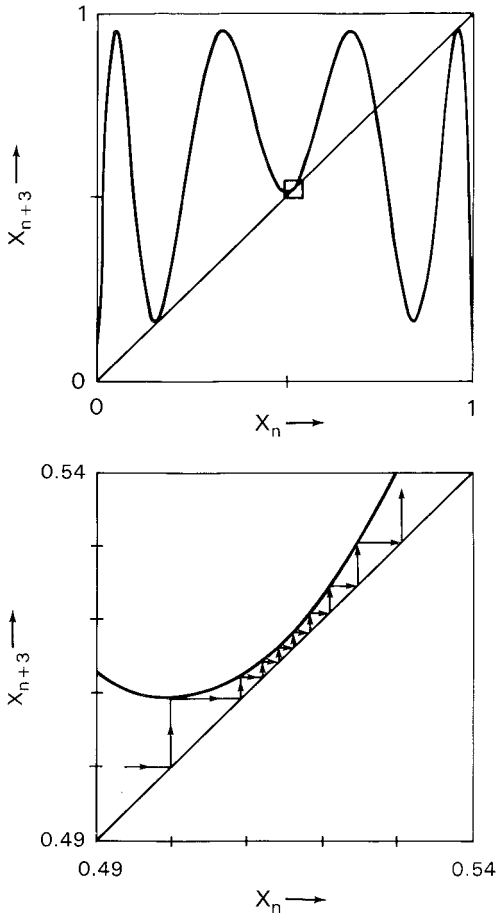

Fig.15: Plot of $f_3(x) = f(f(f(x)))$ at a value of p just below the period 3 window (on the right side of Fig.14a and to the left of Fig.14d). (a) the complete f_3; (b) a blowup of f_3 near $x = \frac{1}{2}$. The fact that many iterations are required to pass through the narrow neck leads to the often-observed phenomenon of "intermittency", in which apparently periodic behavior occasionally appears in the midst of chaos, as in Fig.8e.

process. To do this, Shaw considered a much simpler system—a mass on a spring. The mass, m, represents the whole fluid column, including the growing drop, but in this model the mass is concentrated at a single point at a position y below the equilibrium position (assume downward = positive). The spring produces a linear restoring force equal to $-ky$, where the spring constant k represents surface tension. The mass is subject to a Newtonian friction force $-bv$, where v is the mass's speed,

$$dy/dt = v \tag{22}$$

and b represents friction between the fluid and the faucet. The acceleration of the drop is given by Newton's law:

$$dv/dt = g - (ky + bv)/m, \tag{23}$$

where g is the acceleration of gravity. After a drop breaks off at time $t = t_0$, the mass is assumed to grow as

$$m = m_0 + c(t - t_0), \tag{24}$$

where m_0 is the mass immediately after time t_0 (minus the drop), and c is the mass flow rate. As the mass grows, it may still be oscillating from the previous drop, but eventually dv/dt becomes positive, the mass accelerates downward, the spring stretches, and eventually the next drop breaks off, at say $t = t_1$. For simplicity, the break is assumed to always occur at a fixed location $y = y_0$. Shaw (1984) took the mass of the drop to be proportional to the velocity at the breakpoint, while Scott designed an analog computer which decreased the flow rate by an amount proportional to the distance past the breakpoint, $y - y_0$ (private communication). A simpler rule resets m to m_0 at each breakpoint by simply replacing t_0 by t_1, t_2, etc. in (24). The mass of drop n is then just $c(t_n - t_{n-1})$.

The spring analog of a dripping faucet (for any breakpoint rule) shares with the Bernoulli shift the two essential features of chaos: small changes in initial conditions are amplified over short time intervals, but the solution is confined to a limited region over longer time intervals. The Bernoulli shift amplifies angular differences by doubling them at each iteration, but keeps them limited by dropping the integer part. The spring analog of the dripping faucet amplifies differences in the drop mass because larger drops tend to cause larger rebounds and longer time intervals. This tends to make the next drop larger, but the drop mass is limited because release of a large mass will cause the spring to rebound past its equilibrium point, causing the spring to push in the same direction as gravity, and shorten the time interval and the mass of the next drop. This constant competition between local amplification and global limitation, or between inner freedom and outer constraint, is the essence of chaos.

Discussion

Most of us are familiar with the academic and recreational capabilities of personal computers, but they are also highly sophisticated measuring devices. Some relatively simple plumbing and soldering enables the computer to measure the rapid chaotic rhythms of thousands of drops with accuracies approaching a millionth of a second. The computer becomes a kind of temporal microscope, revealing the marvelous variety of tap dancing going on under the most ordinary leaky faucet. This rich rhythmic behavior creates data clouds of simple spherical and parabolic form, as well as a zoo of complex fractal ribbons not yet fully understood.

These fractal attractor patterns are not only pleasant to the eye, but can also be put to practical use predicting apparently random behavior such as that shown in Figs.5

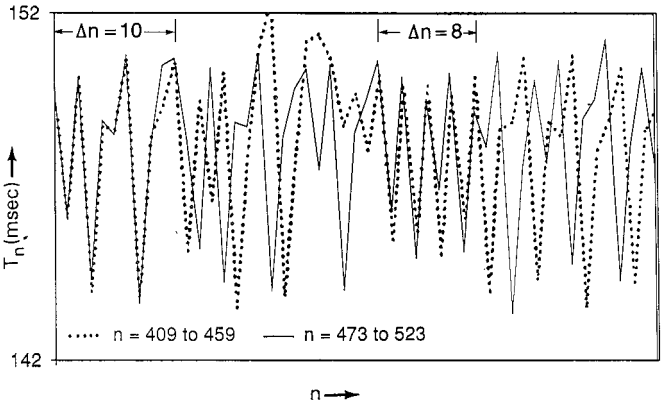

Fig.16: Plot of two 50-drop sequences of time intervals taken from the data in Fig.5c. The starting points were selected by choosing two points nearby on the attractor shown in Fig.7a. The drop intervals remain close together for the first 10 drops, but deviate significantly for drops 11–25, then are back in agreement for drops 26–34, and finally disagree for the remainder. Such behavior shows that analogue prediction schemes, such as those used in short-term weather forecasting, can successfully predict chaotic sequences for a limited time.

and 8. As a simple example, imagine that after collecting drop times in Fig.5c up to drop n = 500, we wish to predict what will happen next. From the previous data, locate points close to (T_n, T_{n+1}) on the attractor in Fig.6c. Each of these points with coordinates (T_m, T_{m+1}), where $m < n$, have successors T_{m+2}, and Fig.7a shows that they provide a good prediction of T_{n+2}. This means that if a pair of drop times is similar to some past pair, what happens next will also be similar for a while. A related procedure called "analog prediction" has occasional success in weather forecasting, and is probably superior to linear statistical prediction since the atmosphere's attractor, like Fig.7a, is expected to be nonlinear (Lorenz, 1977). The atmosphere's nonlinearity leads to the fractal structure of clouds (Cahalan, 1989) just as the dripping faucet's nonlinearity leads to fractal chaotic time intervals.

Fig.16 illustrates the potential predictability inherent in the attractor of Fig.7a by overlaying two such analogs from the middle of Fig.5c, showing that a single past analog can predict a dripping faucet with reasonable accuracy 7–10 drops ahead. Considerable progress is needed before weather can be predicted equally well 7–10 days ahead. In simple systems predictions can be greatly improved by finding each successive interval from a weighted average of a number of neighboring attractor points (Farmer and Sidorowich, 1987; Casdagli, 1989). Such methods are much more difficult to apply in higher-dimensional systems such as weather and climate.

The basic dripping faucet experiment described here can be extended in a number of directions: varying the flu-

id properties, varying the eyedropper properties, varying the environment, and measuring new properties of the dripping process. Wu et al., (1989) and Wu and Schelly (1989) have reduced surface tension by adding the surfactant SDS to the water, producing data clouds whose fractal structure is much clearer, and also finding some new multi-loop patterns. One could also study the effect of fluid density and viscosity, using fluids like oil and mercury. Wu et al. found no strong temperature-dependence for water near room temperature, but what about fluids in temperature ranges where physical properties are changing? Another variable is the shape and size of the eyedropper orifice. What happens if it is covered by a screen? An interesting environmental variation is to apply a constant electric field to the orifice by placing the center of a horizontal copper ring about one ring radius below the eyedropper, and applying a constant voltage. (Earth's ambient field is typically 100V/m downward.) Since water is highly polar, each drop tends to break off with a small net charge, which increases linearly with the applied voltage. Are drop rhythms affected by electric fields? What if the polarizability is altered by, say, changing the salinity?

Besides varying more parameters, we need to refine and extend the measurements. One very useful extension of our photodiode detector would be a camera shutter release triggered by each passing drop. This would generate a movie with the triggering drop in the same position in each frame. Each following drop then appears at a height proportional to the time interval, so that successive frames produce a continuous chaotic dance. A stroboscope can also reveal chaotic patterns, but these are not simply related to the time intervals.

Besides the drop time interval, other useful measurements include the drop diameter and the drop charge. The diameter could be estimated from the drop passage time, determined from the pulse width of the photodiode detector voltage. One way to get the pulse widths is to connect the photodiode detector to an analog-to-digital converter chip (like Radio Shack's TLC548), allowing the complete voltage time series to be recorded digitally. This would require considerable data storage. The charge might be found from the current induced in a conducting ring. Shaw's spring analog model suggests that it would also be of interest to study the recoil of the fluid column resulting from each drop release, to see if it is related to the drop mass or charge. Perhaps this could be done by mounting the eyedropper on a piezoelectric crystal.

Robert Shaw concludes his monograph on the dripping faucet with the hope that his work "suggests that one does not need a particle accelerator to step to the frontiers of physics." We hope even some nonprofessional readers might have that frontier experience, and we have tried to show that it does not necessarily require a well-equipped scientific laboratory, but only access to some relatively common technology.

Acknowledgements: The authors thank Peter Scott for a discussion of analog models, Robert Shaw for encouragement and permission to reproduce the inset in Fig.9a, Ephrem Tekle for providing references and discussing the surface tension effect, Yoram Kaufman and Zoltan Schelly for helpful comments on the manuscript. We are also grateful to John Kavanaugh for discussions on PC data acquisition, John Merritt for generating a movie of the 3D data, Dennis Flanigan for preparation of the bifurcation plot, and Jon Robinson for photographing the drops. ■

References

Batchelor, G. K., 1967, *An Introduction to Fluid Dynamics*, Cambridge University Press, xvii + 615 pp.

Berlin, Howard, 1976, 555 *Timer Applications Sourcebook, with experiments*, Howard W. Sams and Co., 158 pp.

Boys, C. V., 1959, *Soap Bubbles and the forces that mold them*, Doubleday Anchor Books, New York, 156 pp.

Cahalan, Robert F., 1989, "Overview of fractal clouds", in *Advances in Remote Sensing Retrieval Methods*, A. Deepak Pub., pp. 371–389, xxxiv + 519 pp.

Casdagli, Martin, 1989, "Nonlinear prediction of chaotic time series", *Physica D*, **35**, 335–356.

Crutchfield, J. P., J. D. Farmer, N. H. Packard, and R. S. Shaw, 1986, "Chaos", *Sci. Am.*, **255**, 46-57.

Farmer, J. Doyne, and J. J. Sidorowich, 1987, "Predicting chaotic time series", *Phys. Rev. Lett.*, **59**, 845-848.

Feigenbaum, M. J., 1983, "Universal behavior in nonlinear systems", in *Nonlinear Dynamics and Turbulence*, G. I. Barenblatt, G. Iooss and D. D. Joseph, Pitman Advanced Publishing Program, pp. 101–138, 356 pp.

Gleick, James, 1987, *Chaos: making a new science*, Viking Penguin Inc., New York, xi + 32pp.

Hofstadter, Douglas R., 1981, "Strange Attractors: mathematical patterns delicately poised between order and chaos", *Sci. Am.*, **239**, 22–43.

Kaplan, Harvey, 1987, "A cartoon-assisted proof of Sarkowskii's theorem", *Am. J. Phys.*, **55**, 1023-1032.

Lorenz, E. N., 1963, "Deterministic nonperiodic flow", *J. Atmos. Sci.*, **20**, 130–141.

Lorenz, E. N., 1976, "Nondeterministic theories of climate change", *Quat. Res.*, **6**, 495–506.

Lorenz, E. N., 1977, "An experiment in nonlinear statistical weather forecasting", *Mon. Wea. Rev.*, **105**, 590–602.

Mandelbrot, B. B., 1983, *The Fractal Geometry of Nature*, W. H. Freeman and Co., San Francisco, 460 pp.

Martien, P., S. C. Pope, P. L. Scott and R. S. Shaw, 1985, "The chaotic behavior of the leaky faucet", *Phys. Lett.*, **110A**, 399–404.

May, R. M., 1976, "Simple mathematical models with very complicated dynamics", *Nature*, **261**, 459–467.

Mims, Forrest H., III., *Getting Started in Electronics*, Tandy Corporation, 128 pp.

Nelson, A. R., and N. R. Gokhale, 1972, "Oscillation frequencies of freely suspended water drops", *J. Geophys. Res.*, **77**, 2724–2727.

Poincaré, H., 1892-99, *Les Méthodes Nouvelles de la Mécanique Céleste* (3 vols.), Paris: Gauthier-Villars.

Schuster, H. G., 1988, *Deterministic Chaos*, VCH Publishers, Weinheim, FRG, xxiii + 270 pp.

Shaw, Robert, 1984, *The Dripping Faucet as a Model Chaotic System*, Aerial Press, Santa Cruz, CA, 111 pp.

Wisdom, J., 1987, "Chaotic dynamics in the solar system", *Icarus*, **72**, 241–275.

Wu, X., E. Tekle and Z. A. Schelly, 1989, "Dripping faucet apparatus with temperature and high resolution timing and flow rate controls", *Rev. Sci. Instr.*, **60**, 3779–3782.

Wu, X. and Z. A. Schelly, 1989, "The effects of surface tension and temperature on the nonlinear dynamics of the dripping faucet", *Physica D*, **40**, 433–443.

Yepez, H. N. Nuniez, A. L. Salas Brito, C. A. Vargas and L. A. Vicente, 1989, "Chaos in a dripping faucet", *Eur. J. Phys.*, **10**, 99–105.

Listing 1. Program droptime.c.

Compile with Turbo C and TASM or MASM.

```
#include <stdio.h>
#include <alloc.h>
#include <stdlib.h>
#include <conio.h>
#include <ctype.h>
#include <string.h>
#include <dos.h>
#define     NDROPS          1000
#ifdef AT   #define BIT7    128&inportb(0x3BD)
#else       #define BIT7    128&inportb(0x379)
#endif
#define     TICKSPERSEC     1193181.667
#define     LONGS           4,294,967,296.0
void cardinal(long l,double *r)
{*r = ((l<0)?LONGS + (long)l:(long)l);
}
void elapsedtime(long start, long stop, double *t)
{double temp;
cardinal(stop-start, &temp);
*t = (1000.0*temp)/TICKSPERSEC;
}
void initializetimer(void)
{ outportb(0x043,0x034);
  asm jmp short NullJump1
NullJump1:;
  outportb(0x040,0x000);
  asm jmp short NullJump2
NullJump2:;
  outportb(0x040,0x000);
}
void restoretimer(void)
{ outportb(0x043,0x036);
  asm/jmp short NullJump1
NullJump1:;
  outportb(0x040,0x000);
  asm jmp short NullJump2
NullJump2:;
  outportb(0x040,0x000);
}
long readtimer(void)
{ asm cli
  asm mov dx,020h
  asm mov al,00Ah
  asm out dx,al
  asm mov al,00h
  asm out 043h,al
  asm in al,dx
  asm mov di,ax
  asm in al,040h
  asm mov bl,al
  asm in al,040h
  asm mov bh,al
  asm notbx
  asm in al,021h
  asm mov  si,ax
  asm mov al,00FFh
  asm out 021h,al
  asm mov ax,040h
  asm mov es,ax
  asm mov dx,es:[06Ch]
  asm mov ax,si
  asm out 021h,al
  asm sti
  asm mov ax,di
  asm test al,001h
  asm jz done
  asm cmp bx,0FFh
  asm ja done
  asm inc dx
done:;
  asm mov ax,bx
}
void main()
{int dropcount = 0;
long start_t, stop_t;
double *t_p, *first_t_p, *temp_p;
char YNanswer, *datafile, *tempfn;
FILE *f_p;
if((t_p = (double *)
  malloc(NDROPS*sizeof(double))) == NULL)
{     printf("\nNot enough storage !!!");
      exit(0); }
temp_p = first_t_p = t_p;
datafile = (char *)malloc(26);
tempfn = (char *)malloc(26);
initializetimer();
puts("\nHit a key to begin data collection.\n");
while(!kbhit());
getch();
while(BIT7);
start_t = readtimer();
delay(20);
puts("Starting...\n");
while(dropcount <NDROPS && !kbhit()) {
    while(BIT7);
    stop_t = readtimer();
    delay(20);
    elapsedtime(start_t, stop_t, t_p);
    start_t = stop_t;
    t_p++;
    putch('.');
    dropcount++;}
restoretimer();
puts("\nHit a key to view data.\n");
getch();
while(temp_p++<t_p) printf("%10.2f\t",*temp_p);
puts("\nSave data? 'N' to quit, 'Y' to save:\n");
scanf("%c", &YNanswer);
if(toupper(YNanswer)!='N') {
    puts("Insert disk, then hit a key.\n");
    while(!kbhit());
    getch();
    puts("Filename (8 characters or less):");
    scanf("%s", datafile);
    strcpy(tempfn,"a:\\");
    tempfn = strcat(tempfn, datafile);
    datafile = strcat(tempfn, ".dat");
    f_p = fopen(datafile,"wt");
    temp_p = first_t_p;
    while(temp_p++<t_p)
                fprintf(f_p,"%10.2f\n",*temp_p);
    fclose(f_p);
    printf("\nData saved in %s !!!", datafile);}
}
```